Force-Sensing Surgical Grasper Enabled by Pop-Up Book MEMS

Joshua B. Gafford , *Student Member, IEEE*, Samuel B. Kesner, *Member, IEEE*, Robert J. Wood, *Member, IEEE*, Conor J. Walsh, *Member, IEEE*

***Abstract*— The small scale of minimally-invasive surgery (MIS) presents significant challenges to developing robust, smart, and dexterous tools for manipulating millimeter and sub-millimeter anatomical structures (vessels, nerves) and surgical equipment (sutures, staples). Robotic MIS systems offer the potential to transform this medical field by enabling precise repair of these miniature tissue structures through the use of teleoperation and haptic feedback. However, this effort is currently limited by the inability to make robust and accurate MIS end effectors with integrated force and contact sensing. In this paper, we demonstrate the use of the novel Pop-Up Book MEMS manufacturing method to fabricate the mechanical and sensing elements of an instrumented MIS grasper. A custom thin-foil strain gage was manufactured in parallel with the mechanical components of the grasper to realize a fully-integrated electromechanical system in a single manufacturing step, removing the need for manual assembly, bonding and alignment. In preliminary experiments, the integrated grasper is capable of resolving forces as low as 30 mN, with a sensitivity of approximately 408 mV/N. This level of performance will enable robotic surgical systems that can handle delicate tissue structures and perform dexterous procedures through the use of haptic feedback guidance.**

I. Introduction

Minimally-Invasive Surgery (MIS), such as laparoscopic surgery, arthroscopic surgery, and microsurgery, presents a number of significant challenges due to the limited maneuverable workspace and the presence of many delicate structures that must be avoided, including sensitive cartilage surfaces, soft tissue structures, nerves, blood vessels and tendons [1]. Microsurgical procedures, such as nerve or blood vessel anastomosis, are further limited by the challenges of manipulating millimeter-scale and submillimeter-scale tissue structures that are exceedingly fragile and thin. Current commercial MIS instruments are morphologically simple and lack distal articulation or sensing. Additional degrees of freedom and sensing would enable greater access and dexterity and the ability to record and control force applied to the tissue [2]. In addition, the robust electromechanical surgical tools at mm and sub-mm scales required for these procedures are either exceedingly challenging or commercially impractical to make with existing manufacturing techniques such as surface/bulk micromachining [3], wire-EDM [4], micro-injection molding, or micromilling/lathing [5]. It is our goal to apply an emerging micromachining and assembly technique that we have developed to enable robust, dexterous, and practical MIS instruments with integrated sensing.

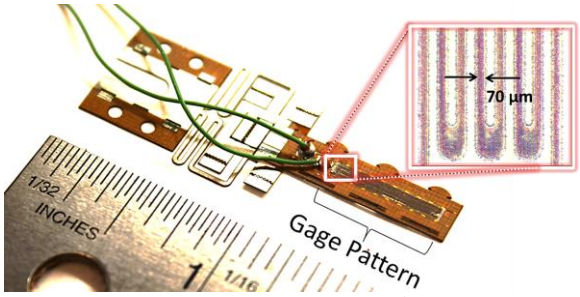

Figure 1. Integrated micrograsper top layer, unfolded, with strain gage embedded in the jaws.

There is a considerable amount of previous work in the area of MIS robotics and force sensing, including end effectors for robot-assisted surgery [6], force sensors for microsurgery [7, 8, 9, 10], and force control approaches to interacting with small-scale tissue structures [11, 12]. Our work differs from the previous work in that it is our goal to fabricate strain and force sensing directly into a robotic end effector in one automated monolithic process, obviating the need for manual integration of fragile or sensitive transducers. To achieve this objective, we have employed and further developed a novel micro manufacturing technique known as Pop-Up Book MEMS ('Pop-Ups') that enables the fabrication of complex, multi-functional electromechanical devices on the 0.1-10 mm scale [13, 14]. Pop-Up technology enables the creation of 3-D, multi-material, monolithic meso and micro-structures using purely 2-D planar manufacturing and origami folding techniques. The method draws upon techniques from printed circuit (PC) board manufacturing, allowing for the straightforward integration of embedded on-board electronics and power (see Figure 1). An example Pop-Up mechanism, featuring 9 layers, joints and springs that allow the structure to 'pop-up' after release cuts are made, is shown in Figure 2.

Our prior work has yielded a cable-driven minimally-invasive surgical grasper prototype manufactured using Pop-Up Book MEMS [15]. The previous grasper, both in flat (post-manufacturing) and 'popped up' (functioning) form, is shown in Figure 2. This grasper was fabricated from medical-grade materials, was robust enough to withstand substantial forces, and was fabricated in one monolithic process. The work presented here builds on the previous

J. G. is with the School of Engineering and Applied Sciences at Harvard University, Cambridge, MA 02138 USA (phone: 817-320-3328; e-mail: jgafford@ seas.harvard.edu).

S.K. is with the Wyss Institute for Biologically Inspired Engineering at Harvard University, Cambridge, MA 02138 USA (e-mail: skesner@seas.harvard.edu).

R.W. and C.W. (corresponding author) are with the Faculty of the School of Engineering and Applied Sciences at Harvard University, Cambridge, MA 02138 USA, and also with the Wyss Institute for Biologically Inspired Engineering, Harvard University, Boston, MA 02115 USA (e-mail: rwood@seas.harvard.edu, walsh@seas.harvard.edu)

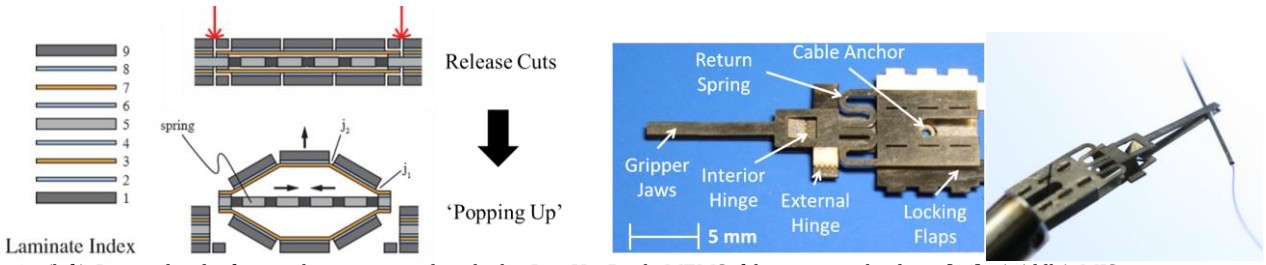

Figure 2. *(left)* Layup detail of a mechanism created with the Pop-Up Book MEMS fabrication technology [14], *(middle)* MIS grasper prototype manufactured via Pop-Up Book MEMS, and *(right)* grasper manipulating a 1.5-gauge straight-taper suture needle.

grasper design to implement strain-based force sensing directly into the grasper layup to create a force-feedback-capable end-effector for teleoperated robotic systems for MIS applications. In the following sections, we present an overview of the manufacturing process used to fabricate this fully-integrated, sensorized grasper followed by an overview of the sensor design process. Results of standalone sensor calibration and characterization tests are presented along with an integrated sensor/grasper that accurately senses distal loads with high resolution.

II. Manufacturing

A. Manufacturing Overview

An overview of the Pop-Up book MEMS fabrication process is illustrated in Figure 3. Beginning with a 2D CAD model of the device, interior and alignment features on each individual layer comprising the layup are machined via laser ablation using a diode-pumped solid-state (DPSS) laser. Each layer is then deburred if necessary and exposed to a two-step cleaning process: (1) Isopropyl Alcohol soak and ultrasonic clean (80º C for 10 minutes) to remove surface-level particulates, and (2) plasma etch with argon gas (0.40 mbar at 2-4 sccm for 60s [16]) to remove contaminants and improve the surface microtexture. The layers are then prepped for lamination and each structural layer is 'back-tacked' to deposit the adhesive islands so that the adhesive protective backing can be removed and disposed of. The entire laminate layup is cured during a two-hour curing process where heat and pressure (60 psi, 200º C) are applied to set the adhesive. Following this step, the layup is released from the surrounding alignment scaffold using the DPSS laser and mechanically 'popped up' to assume the functional form of the prototype. From start to finish, the entire fabrication process takes approximately 10 hours.

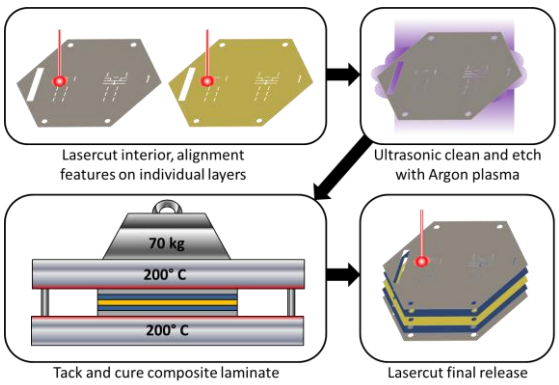

Figure 3. Pop-Up MEMS fabrication process flowchart.

B. Layup Design

A cross-section of the current generation grasper layup is shown in Figure 4. The composite layup for the entire grasper consist of 15 layers of alternating structural, adhesive and flexible layers. The layup consists of 50 µm thick 304 Stainless Steel as the structural layer, 25 µm thick polyimide as the flexible layer, and 5 µm thick gage material integrated directly into the top layer. The layup is bonded using DuPont FR1500 acrylic sheet adhesive.

III. Strain Gage Design and Characterization

A. Gage Design Requirements

The strain gage is designed to detect loads applied to the distal end of the grasper so that force magnitude can be accurately sensed given gage calibration data and a linear elastic assumption. For an example microsurgery application, where the grasper will interact with mm-scale nerves and vessels, the gage is required to sense distal loads up to 1 N with a force resolution of 20 mN [17]. This requirement places an upper-bound on the noise floor of the sensor after signal conditioning.

B. Gage Design and Analysis

Given the design requirements set forth in the previous section, the geometry of the gage pattern can be designed with several considerations in mind. The foremost design challenge is to maximize the gage factor S_e while minimizing the overall footprint:

$$S_e = \frac{\Delta R_s / R_s}{\varepsilon} \tag{1}$$

where R_s is the nominal gage resistance, ΔR_s is the resistance change induced by mechanical deformation, and ε is the material strain. Assuming a linear elastic, isotropic gage material, for a given gage configuration we can express the resistance equation $R = \rho l / A$ as a function of applied strain ε to obtain an analytical model for the change in resistance assuming uniaxial loading:

$$\Delta R_s(\varepsilon) = \rho \sum_{i=1}^{N} \frac{l_i}{w_i t_i} \left(\frac{(1+\varepsilon)}{[(1-\nu\varepsilon)^2]} - 1 \right) \tag{2}$$

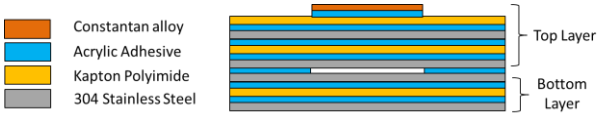

Figure 4. Cross-section of a typical PopUp grasper layup, with gage material integrated into the top layer.

where ρ is the resistivity of the gage material, and ν is the Poisson ratio. Assuming a complex geometry, we have summed resistance contributions from each discrete feature (length l_i, width w_i, and thickness t_i) of the gage pattern. Figure 5 demonstrates the geometry of a discrete element in a more complicated gage pattern.

From Equation (2), the sensitivity of the gage is directly proportional to length l_i and inversely proportional to cross-sectional area $A_{c,i} = w_i t_i$. Serpentine gage patterns typical of commercial off-the-shelf (COTS) metal foil gages are designed to optimize this relationship. For this reason, a serpentine gage pattern was implemented to fit the form factor of the grasper jaw.

Practical machining considerations, such as the DPSS laser tolerance, thermal conductivity of the gage material, and potential inclusion of foreign particulates, limit the smallest achievable feature size to around 50 µm. As such, gage factors (Equation 1) using this process are limited to 1-2 according to Equations (1) and (2).

An additional consideration concerns thermal power dissipation as wasted heat goes towards thermal expansion of the substrate material, which is detrimental to sensor accuracy and long-term stability. Using a lumped impedance model where each material layer separating the gage material from the steel substrate is assigned a thermal impedance (both conductive and convective, see the equivalent circuit in Figure 6 *left*), steel substrate temperature vs. gage resistance was analytically determined to facilitate selection of gage nominal resistance:

$$\mathbf{K}_{6\times6} \cdot \begin{bmatrix} T_{amb} \\ T_g \\ T_{a1} \\ T_k \\ T_{a2} \\ T_{ss} \end{bmatrix} = \begin{bmatrix} Q + K_{g,amb}T_{amb} \\ 0 \\ K_{g,amb}T_{amb} \\ 0 \\ 0 \\ K_{g,amb}T_{amb} \end{bmatrix} \tag{3}$$

where $Q = (V_{cc})^2/4R_s$ is the heat dissipated across the gage (assuming a balanced bridge configuration), $\mathbf{T}_{6\times1}$ is the temperature vector, and $\mathbf{K}_{6\times6}$ is a sparse diagonal matrix comprised of thermal conductivities of each layer in the laminate through which heat is conducted. Solving this linear system of equations for T_{ss} tells us the temperature at the surface of the steel.

A theoretical curve of steel substrate temperature vs. gage resistance is shown in Figure 6 *(right)*. Steady-state temperatures of below 30 ºC are desirable to minimize deviation from ambient, and as such, a gage was designed with a nominal resistance of above 200 Ω.

Given grasper jaw dimensions, the minimum achievable feature size using DPSS laser machining, and thermal considerations, the gage was designed to have a nominal resistance R_s = 270 Ω with a predicted gage factor of S_e = 1.4 using Equations (1) and (2).

C. Manufacturing Methods

Once the gage pattern was designed, it was integrated directly into the manufacturing of the mechanical grasper structure using Pop-Up Book MEMS fabrication. Constantan foil (5 µm thick, 45% Cu, 55% Ni) was chosen as the sensing layer due to its high resistivity (~520x10^{-9} Ω/m),

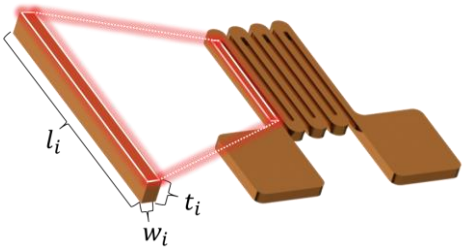

Figure 5. Schematic of discrete element in complicated gage pattern

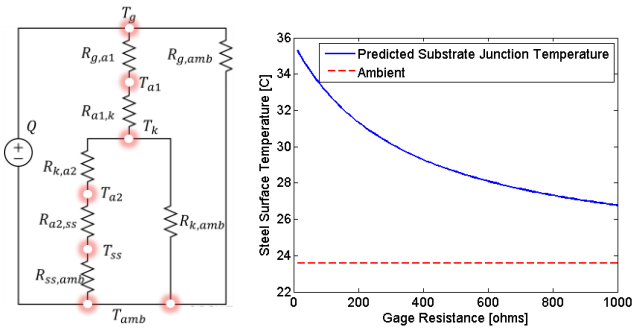

Figure 6. *(left)* Equivalent thermal impedance circuit, and *(right)* theoretical model of 304SS surface temperature vs. gage resistance

versatility, biocompatibility, and comparable thermal expansion (15.0 ppm/ºC) with 304 SS (17.2 ppm/ºC).

The Constantan foil was laminated to the top structural layer of the grasper, as in Figure 7, which shows a conceptual layup of the top grasper jaw. Polyimide provides an extra layer of insulation between the gage and the steel substrate.

The delicate nature of the thin Constantan film yields special processing considerations. The strain gage is machined and laminated in parallel with the mechanical structure, and as a result, the gage material experiences significant thermal gradients (~200º C) during lamination. The residual stress σ_{therm} induced on the gage material during the lamination process can be calculated using a thin-film approximation by assuming the thermal behavior is dominated by the steel substrate:

$$\sigma_{therm} = \frac{E_{const}}{(1-\nu_{const})}(\alpha_{T,const} - \alpha_{T,s})\Delta T \tag{4}$$

where E_{const} is the Young's Modulus of Constantan (169 GPa), ν_{const} is the Poisson ratio (0.33), $\alpha_{T,const}$ is the thermal expansion coefficient for Constantan (15 ppm/ºC), $\alpha_{T,s}$ is the thermal expansion coefficient for 304 SS (17.2ppm/ºC), and ΔT is the process temperature gradient. Based on these parameters, the thermal stresses σ_{therm} induced via lamination are on the order of 166 MPa, resulting

Figure 7. Gage layup on the top structural layer

in a safety factor of about 3 (given $\sigma_y = 500$ MPa for Constantan) demonstrating that thermal stressed induced during the manufacturing process will not result in failure.

After the gage material was laminated directly onto the grasper layup, the serpentine gage pattern was machined into the Constantan foil during the release step following the full cure. At this point, the foil is already fully bonded to the polyimide insulating layer, so the depth of cut must be closely controlled such that the insulating layer is not ablated by the laser, providing a conductive path to the steel substrate.

D. Signal Conditioning

Following successful manufacture of the gage material integrated to the structural substrate, the gage forms one leg of a Wheatstone bridge with tunable balance to account for gage manufacturing variations. The output of the bridge is amplified via a differential operational amplifier (LM741CN) with a gain of 500. Data is then acquired via an Analog-to-Digital Converter (ADC) and passed to the host PC through a serial interface at a sampling rate of 500 Hz.

Assuming a perfectly balanced bridge, the relationship between gage resistance change and output voltage is given by Equation (5).

$$\Delta V_{out} = G V_{cc} \left[\frac{R_s}{2R_s + \Delta R_s} - \frac{1}{2} \right] \tag{5}$$

This amplification circuit boosts fractional gage resistance changes to measurable voltages such that strains are resolved with much higher resolution.

E. Gage Characterization

Using the manufacturing process outlined in Section III.C, sample gages were manufactured onto 5 mm by 30 mm 304SS beam substrates with 100 µm thickness for gage characterization. The simple geometry allows for a more straightforward strain characterization based on linear elastic principles.

The average nominal resistance of the manufactured gages is 278±7.16Ω (95% confidence for 6 samples), which is close to the design resistance of 270 Ω computed using Equation (2). The steady-state operating temperature, measured using a thermocouple and data logger, was measured to be approximately 6.5 ºC above ambient, which agrees with the predicted value of 6.85 ºC obtained via thermal impedance modeling (Equation (3)).

Two tests were performed to validate gage performance. For the first test, gages were secured to a benchtop in a cantilever fashion, and discrete weights of known mass were hung on the distal end (Figure 8 (a)). The resulting change in voltage was recorded, and ΔR_s was solved for using Equation (5). The strain was calculated as follows:

$$\varepsilon = \frac{mgcL}{E_s I} \tag{6}$$

where m is the load mass, g is the universial gravitational constant, c is the distance separating the location of maximum stress (at the gage surface) from the neutral axis of the beam, L is the length along the beam where the load is hung, E_s is the Young's modulus of 304 SS and I is the second moment of area.

The second characterization approach was experimentally more rigorous but enables an even simpler model to compute strain. Using an Instron tensile testing machine with a static load cell (Figure 8 (b) and (c)), gage samples were loaded in uniaxial tension over a triangular force profile (4 N/s) up to approximately 50% of σ_y, corresponding to a maximum tensile load of 200N (See Figure 8a and 8b). Data were collected at a rate of 500 Hz and post-processed in MATLAB. In the case of composite uniaxial tension, and accounting for elasticity in the polyimide layer, the strain is computed as:

$$\varepsilon = \frac{F}{(A_k E_k + A_s E_s)} \tag{7}$$

where A_k, A_s E_k and E_s denote cross-sectional areas and Young's moduli for polyimide and 304SS, respectively. It is assumed that the adhesive layers don't contribute significantly to the deformation of the substrate.

Results of the tests are shown in Figure 8 (d). It is clear that both methods yield consistent results. However, measured ΔR_s *vs.* ε deviates from the trend predicted via Equation (2) and the anticipated gage factor of S_e= 1.4. This is likely a result of unmodeled effects, such as shear deformation in the adhesive layer. The measured gage factor is 1.1, which is a typical number for thin metal foil gages.

F. Thermal Sensitivity

In addition to mechanical characterization, the thermal characteristics of the gage must be adequately determined to quantify stability of the sensing system when operating in environments with varying temperatures. The thermal expansion of the steel structural material induces strain in the gage material, resulting in resistance drifts as a function of temperature. Recalling Equation (2), and replacing

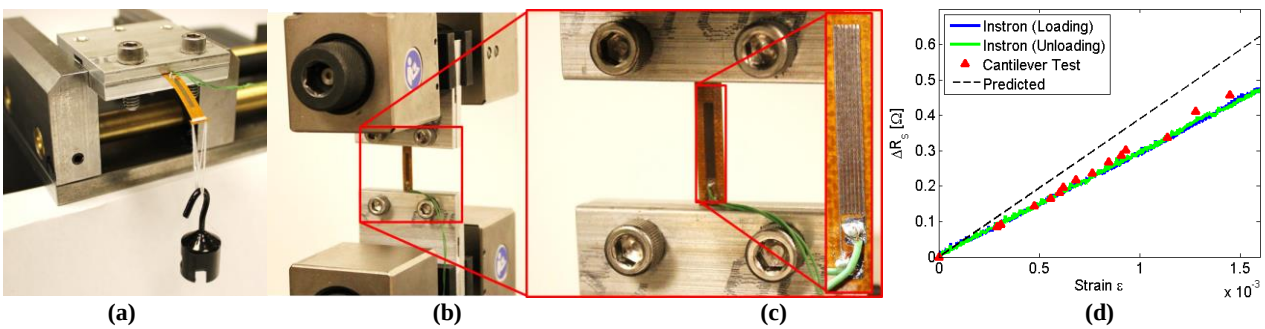

(a) **(b)** **(c)** **(d)**

Figure 8. (a) Cantilever gage characterization setup, (b) Instron characterization setup, (c) closeup of gage undergoing testing, and (d) calibration results compared with theoretical prediction, demonstrating the measured gage factor of 1.1.

mechanical strain with thermal strain ($\varepsilon_{therm} = \alpha\Delta T$) the change in resistance due to temperature gradients can be computed via:

$$\Delta R_s(\Delta T) = \rho \sum_{i=1}^{N} \frac{l_i}{w_i t_i}\left(\frac{(1+\alpha\Delta T)}{[(1-\nu\alpha\Delta T)^2]} - 1\right) \quad (8)$$

Experimental data was collected to compare to the analytical model described by Equation (8). Gages were heated on a hot plate, instantaneous temperature was recorded with a thermocouple and datalogger, and the resistance was recorded using a digital ohmeter. The theoretical model from Equation (8) is plotted along with the experimental data in Figure 9. The sensors demonstrate a sensitivity of 7.1 mΩ/ºC. Plugging into Equation (5) the voltage sensitivity is $G \cdot 31.7\ \mu V/$ºC where G is the differential gain. In an anatomical setting, temperature gradients of up to 15 ºC can be expected, resulting in a voltage swing of over 200 mV for 500 gain. Therefore, inclusion of a temperature-compensating gage is desirable and relatively trivial to implement in future designs.

G. Failure Modes

Observed failure modes can be categorized into overloading failures and manufacturing failures. Representative optical microscope images of both of these failure modes are shown in Figure 10. Manufacturing failures are process failures that occur when foreign particles are introduced underneath the gage material during pre-lamination resulting in gage material yielding and puncture during the lamination pressing process. Overloading failures are operational failures that occur when the gage material mechanically yields at high strain or high fatigue, breaking the conductive path.

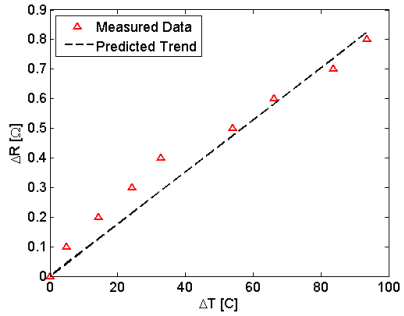

Figure 9. Gage sensitivity to thermal gradients.

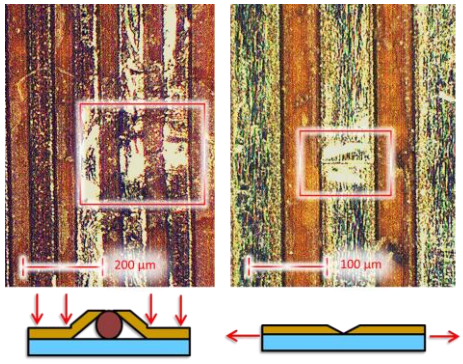

Figure 10. Observed failure modes: *(left)* Particulate contamination in the laminate resulting in yielding. *(right)* overtension

IV. Integrated MIS End Effector with Sensing

To demonstrate the efficacy of embedded strain sensing in an integrated platform, a 2:1 scale MIS end-effector with the strain gage directly integrated was fabricated using the PopUp manufacturing process outlined in Section II. The gage was fabricated in parallel using the same process, yielding a fully-integrated force-sensing end-effector with no post-manufacturing bonding, alignment or gage assembly required.

A. Mechanical Design

The mechanical design of the basic grasper is detailed in [15]. The design was improved structurally by incorporating 3-dimensional features that fold out of plane and lock into place to increase jaw stiffness over a planar jaw with no out-of-plane features (see illustration in Figure 11). If we consider bending about the x-axis as defined in Figure 11, we can compute the second moment-of-area J_{xx} of the folded-over jaw as follows:

$$J_{xx} = \frac{bh^3}{12} - \frac{(b-2t)(h-2t)^3}{12} \quad (9)$$

where *b*, *h*, and *t* are as defined in Figure 11. Comparing to a 2D planar jaw where $J_{xx} = bt^3/12$, the stiffness is improved by over 200 times given *b*=2mm, *h*=1mm and *t*=150µm.

A flexural return spring is placed in line with the cable actuation force, and is designed to remain elastic over the 4mm range of motion that comprises the grasper's overall travel while providing sufficient restoring force to overcome gravity and hinge friction. The result is a pure parallel closing motion, with castellated hinges acting as rotary bearings to constrain any transverse motion. Previous studies have shown these castellated hinges to resist torsional loads of 22.8±2.15 N·mm per mm of hinge width, and given four 3mm wide hinges, the grasper is expected to endure maximum tip loads of around 4 N which provides a significant factor-of-safety over the design load of 1 N.

B. Gage Design and Integration

The gage is completely enveloped by the fold-over jaw design, which serves to both physically isolate the gage from the environment, and provide protection against stray capacitance via the Faraday Cage effect. Additional insulation can be provided by potting the gage area with an epoxy. Solder pads are encompassed entirely inside the foldable jaw, so there are no exposed leads. The stiffness of the jaws is substantially higher than that of the sample beams used for gage characterization, so the gain of the

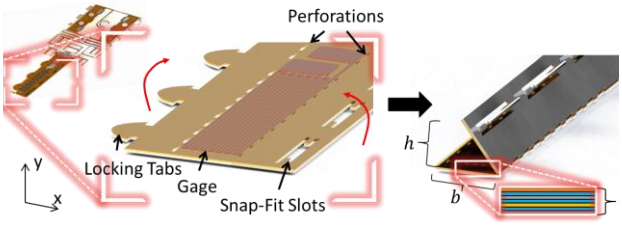

Figure 11. Illustration of foldable flaps to insulate the gage and improve mechanical stiffness of grasper jaw.

amplifier circuit was increased from 500 to 1650. RMS noise from the circuit is on the order of 15 mV.

Images of the integrated grasper, both post-release ('unpopped') state and partially popped with the jaw folded over to insulate the gage, are shown in Figure 12.

C. Evaluation

The static performance of the integrated grasper was evaluated in a similar manner as the standalone gage. Benchtop cantilever tests yielded the results presented in Figure 13 *(left)*. From this characterization data, the sensitivity can be shown to follow a linear trend of approximately 458 mV/N. Considering the RMS noise of 15 mV caused by the high-gain differential amplifier, the sensor can detect loads of upwards of 33 mN, which is very close to the design requirement of 20 mN resolution.

The grasper was also characterized in a dynamic setting by providing time-varying distal loads using an Instron tensile testing machine with a 10 N static load cell. A loading profile resulting in the response shown in Figure 13 *(middle)*. The observed sensitivity from the dynamic profile is around 408 ± 4 mV/N (95% Confidence). The error results from some minor but observable hysteresis between loading/unloading intervals, which can be seen in Figure 13 *(right)*.

Figure 14 shows images of the grasper undergoing a simulated manipulation task, along with the force signals (raw data and filtered via 2nd-order Butterworth filter)

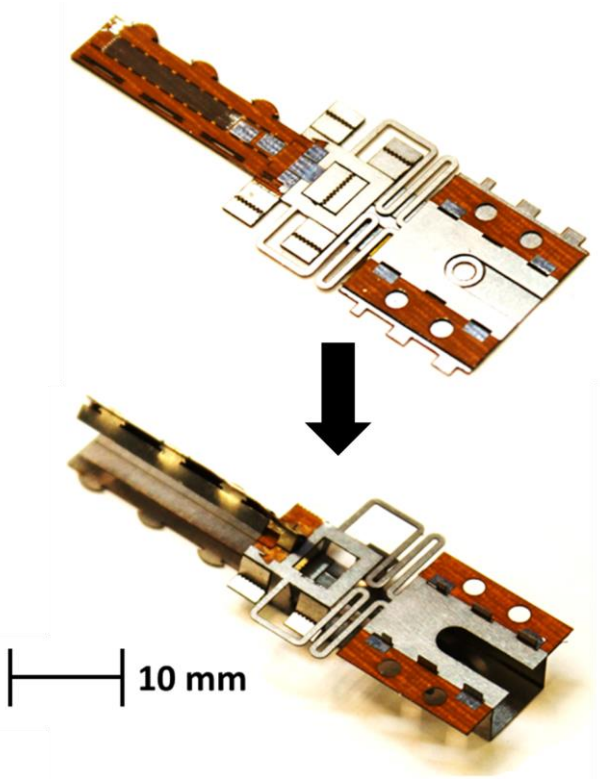

Figure 12. Force-sensing micrograspers: Post-release cut, unpopped (top) and popped up with the top jaw folded over to insulate the gage

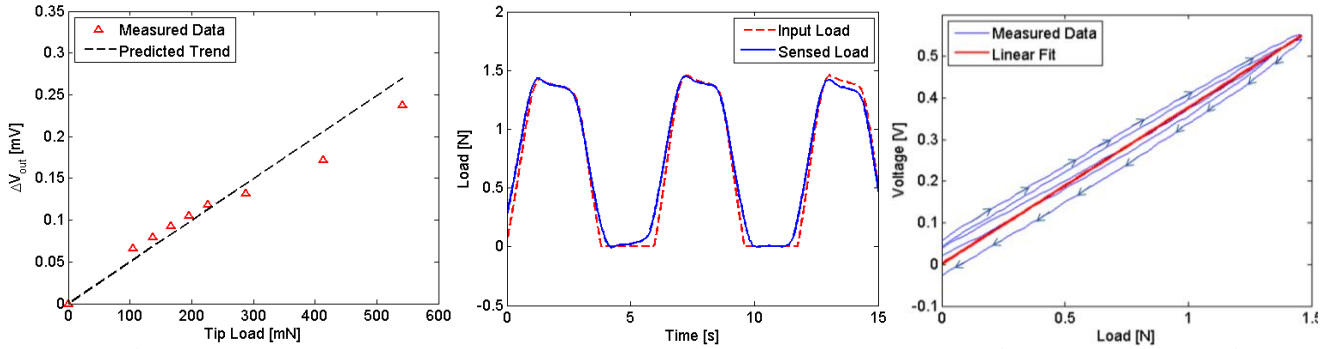

Figure 13. *(left)* Static characterization results, *(middle)* integrated system response to dynamic loading profile, and *(right)* results of dynamic characterization, showing slight hysteresis but an overall linear response.

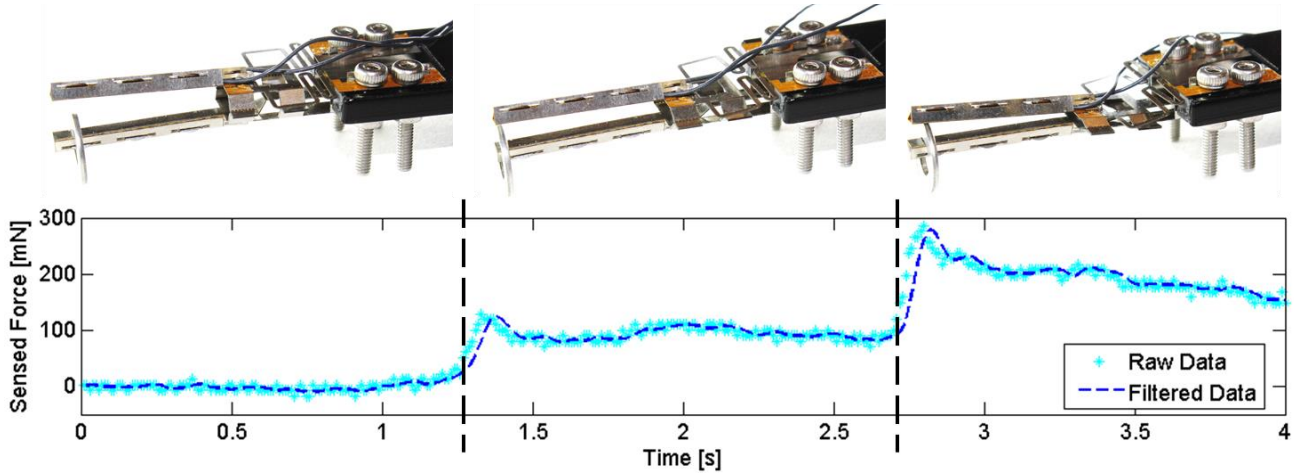

Figure 14. Integrated sensor performance during object manipulation task: *(left)* unloaded grasper showing a null force reading, *(middle)* light contact with object registering ~100 mN, and *(right)* larger force peaking at nearly 300 mN.

generated throughout the task. The grasper was able to distinguish between states of no-load, initial contact or light-load, and heavy-load. The overshoot at each loading phase is due to the deformation of the flexural return spring which, in addition to providing mechanical damping in the system, initiates a second-order response.

V. A Note on Biocompatibility

The planar nature of the device 'pre-popped' allows for straightforward deposition of a Parylene coating which will encapsulate the device with a biocompatible coat. In addition, we are working closely with an industrial collaborator to develop a heat- and pressure-activated biocompatible adhesive (in sheet form) to substitute into the layup. The other constituent materials (304 SS and polyimide) are already biocompatible. The low overhead cost of materials and labor makes the gripper an economical candidate for single-use, thus obviating the need for sterilization.

VI. Conclusions and Future Work

We have presented a novel surgical grasper prototype with embedded strain sensing, fabricated entirely using a one-step Pop-Up Book MEMS manufacturing approach. The grasper was experimentally shown to detect distal loads as low as 30 mN, with a sensitivity of 408 mV/N. Simple manipulation tasks show that the grasper can reliably differentiate between different loading conditions. We envision a large number of applications for this technology in minimally invasive surgical procedures, including microsurgery and small-joint arthroscopy.

Future design iterations will include downscaling by a factor of two to produce a grasper with 1x10mm jaws. We will also integrated cutaneous tactile sensing to decouple force localization and magnitude measurements. Integrating multiple sensing modalities with miniature mechanical end-effectors offers the potential to create smart surgical tools that provide physicians with information that enables them to perform more effective and safe procedures. Future work will involve integrating the gripper into minimally invasive tools and evaluating it in realistic clinical settings.

Acknowledgment

The authors would like to acknowledge the Wyss Institute for Biologically-Inspired Engineering and the Harvard School of Engineering and Applied Sciences for their support of this work.

References

[1] R. Berger, "Small-Joint Arthroscopy in the Hand and Wrist," in *Wrist Arthroscopy*, New York, Springer, 2005, pp. 155-166.

[2] U. Seibold, B. Kuebler, H. Weiss, T. Ortmaier and G. Hirzinger, "Sensorized and Actuated Instruments for Minimally Invasive Robotic Surgery," in *EuroHaptics*, Munic, Germany, 2004.

[3] W. Chang and D. Sretavan, "Microtechnology in Medicine: The Emergence of Surgical Microdevices," *The Congress of Neurological Surgeons*, vol. 54, pp. 137-47, 2007.

[4] M. Murali and S. Yeo, "Rapid Biocompatible Micro-Device Fabrication by Electro-Discharge Machining," *Biomedical and Microdevices*, 2004.

[5] J. B. Gafford, M. A. Cullinan, R. M. Panas and M. L. Culpepper, "Design Principles and Best-Practices for Rapid Prototyping Mesoscale Nanopositioers using a Micromill," in *ASPE Annual Meeting*, Atlanta, GA, 2010.

[6] Y. Park, S. Elayaperumal, S. Ryu, B. Daniel, J. Black, B. Moslehi and M. Cutkosky, "MRI-compatible Haptics: Strain sensing for real-time estimation of three dimensional needle deflection in MRI environments," in *International Society for Magnetic Resonance in Medicine (ISMRM)*, Honolulu, HI, 2009.

[7] Y. Park, K. Chau, R. Black and M. Cutkosky, "Force Sensing Robot Fingers using Embedded Fiber Bragg Grating Sensors and Shape Deposition Manufacturing," in *IEEE ICRA*, 2007.

[8] B. Gonenc, M. Balicki, J. Handa, P. Gehlbach, C. Riviere, R. Taylor and I. Iordachita, "Preliminary evaluation of a micro-force sensing handheld robot for vitreoretinal surgery," in *IEEE IROS*, Vilamoura, Portugal, 2012.

[9] I. Iordachita, Z. Sun, M. Balicki, J. Kang, S. Phee, J. Handa, P. Gehlbach and R. Taylor, "A sub-millimetric, 0.25 mN resolution fully integrated fiber-optic force-sensing tool for retinal microsurgery," *International Journal of Computer Assisted Radiology and Surgery*, vol. 4, no. 4, pp. 383-390, 2009.

[10] A. Menciassi, A. Eisinberg, C. Carrozza and P. Dario, "Force sensing microinstrument for measuring tissue properties and pulse in microsurgery," in *IEEE/ASME Transactions on Mechatronics*, 2003.

[11] W. Ang, C. Rivere and P. Khosla, "Design and implementation of active error canceling in hand-held microsurgical instrument," in *IEEE/RSJ International Conference on Intelligent Robots and Systems*, Maui, HI, 2001.

[12] R. Taylor, "A Steady-Hand Robotic System for Microsurgical Augmentation," *The International Journal of Robotics Research*, vol. 18, no. 12, pp. 1201-1210, 1999.

[13] P. Sreetharan, J. Whitney, M. Strauss and R. Wood, "Monolithic Fabrication of Millimeter-Scale Machines," *J. Micromech. Microeng.*, vol. 22, no. 055027, 2012.

[14] J. Whitney, P. Sreetharan, K. Ma and R. Wood, "Pop-Up Book MEMS," *J Micromech. Microeng*, vol. 21, no. 115021, 2011.

[15] J. Gafford, S. Kesner, R. Wood and C. Walsh, "Microsurgical Devices by Pop-Up Book MEMS," in *ASME/IDETC: Robotics and Mechanisms in Medicine*, Portland, Oregon, 2013.

[16] N. Inagaki, "Plasma Graft Copolymerization," in *Materials Surface Processing by Directed Energy Techniques*, Oxford, UK, Elsevier, 2006, pp. 702-07.

[17] F. Hammond III, R. Kramer, Q. Wan, R. Howe and R. Wood, "Soft Tactile Sensor Arrays for Micromanipulation," in *Proc. of 2012 IEEE Int. Conf. on Intelligent Robots and Sensors*, Vilamoura, Portugal, 2012.